

# SDF-Net: Structure-Aware Disentangled Feature Learning for Optical–SAR Ship Re-Identification

Furui Chen, Han Wang, Yuhan Sun, Jianing You, Yixuan Lv, Zhuang Zhou, Hong Tan, and Shengyang Li

**Abstract**—Cross-modal ship re-identification (ReID) between optical and synthetic aperture radar (SAR) imagery is fundamentally challenged by the severe radiometric discrepancy between passive optical imaging and coherent active radar sensing. While existing approaches primarily rely on statistical distribution alignment or semantic matching, they often overlook a critical physical prior: ships are rigid objects whose geometric structures remain stable across sensing modalities, whereas texture appearance is highly modality-dependent. In this work, we propose SDF-Net, a Structure-Aware Disentangled Feature Learning Network that systematically incorporates geometric consistency into optical–SAR ship ReID. Built upon a ViT backbone, SDF-Net introduces a structure consistency constraint that extracts scale-invariant gradient energy statistics from intermediate layers to robustly anchor representations against radiometric variations. At the terminal stage, SDF-Net disentangles the learned representations into modality-invariant identity features and modality-specific characteristics. These decoupled cues are then integrated through a parameter-free additive residual fusion, effectively enhancing discriminative power. Extensive experiments on the HOSS-ReID dataset demonstrate that SDF-Net consistently outperforms existing state-of-the-art methods. The code and trained models are publicly available at <https://github.com/cfrfree/SDF-Net>.

**Index Terms**—Modality disentanglement, optical–SAR ship re-identification, physics-guided representation learning, structure-aware feature alignment.

## I. INTRODUCTION

**O**PTICAL and Synthetic Aperture Radar (SAR) sensors play complementary roles in maritime surveillance. Optical imagery provides rich visual details under favorable illumination, whereas SAR, as an active sensing modality, enables all-weather and day-night observation by measuring microwave backscatter. Integrating these heterogeneous

This work was supported by the Strategic Priority Research Program of the Chinese Academy of Sciences under Grant XDA0360303. (Corresponding author: Shengyang Li.)

Furui Chen, Han Wang, Yuhan Sun, Jianing You, Hong Tan, and Shengyang Li are with the Technology and Engineering Center for Space Utilization, Chinese Academy of Sciences, Beijing 100094, China, also with the Key Laboratory of Space Utilization, Chinese Academy of Sciences, Beijing 100094, China, and also with the University of Chinese Academy of Sciences, Beijing 100049, China (e-mail: chenfurui24@mailsucas.ac.cn; wanghan221@mailsucas.ac.cn; sunyuhuan21@mailsucas.ac.cn; youjianing24@csu.ac.cn; tanhong@csu.ac.cn; shyli@csu.ac.cn).

Yixuan Lv is with the Technology and Engineering Center for Space Utilization, Chinese Academy of Sciences, Beijing 100094, China, and also with the Key Laboratory of Space Utilization, Chinese Academy of Sciences, Beijing 100094, China, and also with the School of Software, Beihang University, Beijing 100191, China (e-mail: lvyixuan@csu.ac.cn).

Zhuang Zhou is with the Technology and Engineering Center for Space Utilization, Chinese Academy of Sciences, Beijing 100094, China, and also with the Key Laboratory of Space Utilization, Chinese Academy of Sciences, Beijing 100094, China (e-mail: zhouzhuang@csu.ac.cn).

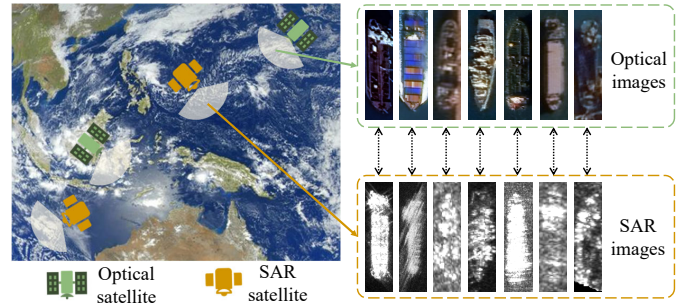


Fig. 1. Illustration of the optical–SAR ship re-identification task. The framework aims to match the same ship identity across vastly different optical and SAR sensor modalities.

sources is therefore critical for continuous ship monitoring and long-term target tracking [1]. As a fundamental component of this integration, cross-modal ship re-identification (ReID) aims to associate ship identities across optical and SAR imagery [2], [3].

However, optical–SAR ReID remains highly challenging due to the intrinsic physical disparity between the two sensing mechanisms. This massive modality gap induces complex non-linear radiometric distortion (NRD) [4], characterized by fundamentally inconsistent intensity responses across sensors due to the vast wavelength difference between microwave backscattering and visible reflectance. Consequently, traditional feature alignment predicated on metric-based distance becomes mathematically ill-posed, as direct appearance correspondence is corrupted by modality-specific signal fluctuations rather than simple Gaussian noise [5]. While optical images capture passive reflectance patterns governed by illumination and material properties, SAR imagery is fundamentally dominated by coherent scattering effects and speckle noise. Texture appearance thus exhibits severe modality-specific distortion, a challenge extensively documented in radar-based ship analysis [6], rendering direct appearance alignment unreliable and often misleading.

Most existing approaches address this challenge from a data-driven perspective, formulating cross-modal ReID as a feature distribution alignment problem [7], [8]. Early works focus on learning a shared embedding space to reduce modality gaps, while recent deep models leverage convolutional neural networks or Vision Transformers (ViT) to implicitly align high-level semantic representations [9]. Although these methods achieve encouraging performance, they typically treat feature extraction as a black-box process and lack explicit mechanisms to distinguish modality-invariant identity cues from sensor-specific interference such as speckle, sea clutter,

or illumination variations.

To further mitigate modality discrepancy, prevailing research has explored generative synthesis and intricate distribution matching strategies [10], [11]. Although these approaches reduce statistical divergence, they frequently impose prohibitive computational costs and risk introducing hallucinatory artifacts that obscure identity-critical features [12]. Critically, such purely statistical alignment overlooks the physical constraints of maritime targets as rigid bodies. In contrast to pedestrian re-identification—which typically exploits deformable pose alignment or stable anatomical proportions [7]—maritime targets exhibit strong intrinsic geometric rigidity. We recognize that SAR imaging inherently introduces projection distortions such as layover and foreshortening under varying incidence angles [2]. However, while these radar-specific phenomena alter micro-level pixel correspondences, the macro-topological layout, global hull proportions, and superstructure configurations of the ship maintain a high degree of cross-modal consistency, particularly under the overhead (near-vertical) observation perspectives typical in satellite remote sensing. Within this near-nadir sensing environment, the macroscopic geometric skeleton provides a robust and distortion-tolerant physical invariant, serving as a definitive anchor for cross-modal representation alignment.

We argue that a more principled solution should directly leverage geometric structure as the common denominator between optical and SAR imagery. For ships, attributes such as hull contour, aspect ratio, and spatial layout are largely invariant across modalities, whereas texture patterns are inherently sensor-dependent. Therefore, enforcing strict consistency on geometric structure while allowing flexibility in modality-specific appearance is crucial for reliable cross-modal ReID. From a representation learning perspective, such geometric information is neither best captured at the raw pixel level nor at highly abstract semantic layers. Instead, it is preserved in intermediate network representations that retain spatial organization while being sufficiently abstracted from low-level noise. This observation motivates us to formally model and constrain structural consistency at intermediate feature layers, rather than relying on implicit alignment at the output level.

Based on these insights, we propose **SDF-Net**, a Structure-Aware Disentangled Feature Learning Network for optical–SAR ship re-identification. Built upon a ViT backbone, SDF-Net introduces a Structure Consistency Constraint to enforce cross-modal geometric alignment at intermediate stages.

At the terminal stage, SDF-Net further decouples the learned representations into modality-invariant shared features and modality-specific features [13]. To effectively integrate these complementary components, we employ an additive fusion strategy, where modality-specific features act as a residual refinement to the shared identity representation. This simple yet effective design avoids feature redundancy and preserves discriminative identity information without introducing additional computational overhead.

In this paper, the term “physics-guided” refers to the direct integration of the physical properties of maritime targets and sensor mechanisms into the network design. First, exploiting the physical prior that ships are rigid bodies, we

introduce a Structure Consistency Constraint to anchor the cross-modal alignment on the invariant geometric hull rather than highly variable textures. Second, to address the distinct physical imaging mechanisms—specifically, the high-intensity dynamic range of SAR coherent scattering versus the narrow-band diffuse reflectance of optical sensors—we apply instance normalization to the gradient energy. This mathematically standardizes the disparate amplitude responses into a modality-agnostic structural descriptor, forming a cohesive physics-informed representation learning paradigm.

The main contributions of this work are summarized as follows:

- We propose SDF-Net, a physics-guided representation learning framework for optical–SAR ship re-identification, which moves beyond implicit statistical matching by firmly anchoring cross-modal association on invariant geometric structures.
- We introduce a scale-invariant structure consistency constraint based on normalized gradient energy statistics from intermediate Transformer layers, enabling highly robust alignment against severe radiometric distortions.
- We design a disentangled feature learning and additive fusion strategy that seamlessly integrates modality-specific residual information into shared identity representations in a completely parameter-free manner.
- Extensive experiments on the HOSS-ReID dataset [3] demonstrate that the proposed method achieves state-of-the-art performance, thoroughly validating the efficacy of physics-guided disentanglement for maritime target association.

## II. RELATED WORK

In this section, we review research efforts closely related to the proposed SDF-Net, organized into three research streams: cross-modal re-identification, disentangled and structure-aware representation learning, and optical–SAR ship analysis.

### A. Cross-Modal Re-Identification

Cross-modal re-identification (ReID) has undergone extensive development within the framework of visible–infrared person ReID (VI-ReID), which focuses on mitigating the distribution gaps between heterogeneous sensors through the acquisition of modality-robust representations [7]. While early methodologies primarily treated modality discrepancy as noise to be suppressed within a shared embedding space, more recent investigations suggest that modality-specific information contains vital discriminative cues that can be selectively preserved to refine identity representations under appropriate constraints [14].

To address spatial misalignment and local correspondence ambiguity, semantic alignment and affinity reasoning mechanisms have been employed to aggregate consistent local regions across disparate manifolds [15]. Furthermore, the emergence of multimodal contrastive paradigms has facilitated the alignment of cross-modal positive pairs by pulling them together within a unified hypersphere manifold [16]. In parallel, structural priors have been integrated into Transformer-based

architectures to safeguard spatial integrity across modalities [17]. However, such structural modeling is typically optimized for articulated human bodies or predicated on high-level semantic correspondence, which proves insufficient when confronting the severe non-linear radiometric differences inherent in optical–SAR imaging.

Notably, the design principles of VI-ReID are not directly transferable to optical–SAR ship ReID due to fundamental differences in object properties and sensing mechanisms. In VI-ReID, human bodies exhibit significant pose and articulation variations, while appearance attributes such as clothing color and texture remain relatively stable across modalities [18]. Consequently, many VI-ReID methods emphasize pose alignment or part-level correspondence to handle structural deformation.

In contrast, ships are rigid objects whose geometric configurations remain largely consistent across viewpoints and sensing modalities, whereas their radiometric appearance undergoes drastic changes due to the distinct physical imaging processes of optical and SAR sensors [2], [19]. The coherent scattering mechanism of SAR often produces bright responses unrelated to optical texture patterns, leading to severe cross-modal appearance inconsistency. Therefore, instead of focusing on pose alignment, optical–SAR ship ReID demands mechanisms that explicitly preserve geometry while tolerating modality-dependent radiometric variations.

### B. Disentangled and Structure-Aware Learning

Disentangled representation learning seeks to decouple identity-relevant information from modality-dependent variations. In the general re-identification (ReID) domain, generative and factorized models have been employed to separate structural content from appearance attributes [13]. While feature disentanglement has been extensively explored in visible-infrared person ReID (VI-ReID) architectures like Hi-CMD [20], these mature strategies cannot be trivially adapted to optical–SAR ship ReID. VI-ReID fundamentally aims to decouple deformable human poses from modality-specific clothing colors under similar passive imaging mechanisms. In stark contrast, maritime targets are rigid bodies, yet their cross-modal discrepancy stems from severe non-linear radiometric distortions caused by distinct physical imaging mechanisms (i.e., active microwave coherent scattering versus passive diffuse reflectance). Consequently, rather than discarding the modality-specific feature  $\mathbf{f}_{sp}$  as mere style noise as commonly practiced in VI-ReID, our approach uniquely treats  $\mathbf{f}_{sp}$  as a physical sensor footprint (e.g., SAR corner reflector responses) and preserves it via an additive residual fusion to complement the rigid geometric skeleton  $\mathbf{f}_{sh}$ . For instance, hierarchical cross-modal disentanglement architectures [20] have demonstrated substantial efficacy in formally factorizing representations into modality-invariant identity features and modality-specific style codes. However, while shape-erased or pose-invariant representations have proven effective for articulated objects such as humans, these assumptions are less applicable to rigid targets. For ships, geometric structure remains largely invariant across viewpoints and sensing

modalities, providing a reliable anchor for cross-modal alignment. Furthermore, the integration of Instance Normalization (IN) has been demonstrated to effectively filter out modality-related “style” variations while preserving essential content information [21].

Beyond disentanglement and normalization-based strategies, recent studies have highlighted the importance of intermediate feature statistics for cross-domain alignment. In neural style transfer, Gram matrix statistics extracted from intermediate convolutional layers are shown to effectively characterize structural and style information [22]. Similarly, feature-level statistical matching has been employed to enforce domain consistency by aligning intermediate representations rather than solely relying on output embeddings [23].

These findings suggest that intermediate layers preserve spatial organization and structural cues that are partially invariant to low-level appearance variations. Inspired by this line of research, we specifically extract normalized gradient energy statistics from intermediate Transformer layers to construct scale-invariant structural descriptors for cross-modal ship ReID.

Nevertheless, completely discarding modality-specific characteristics may lead to the loss of fine-grained discriminative details. This has prompted recent studies to investigate the integration of explicit geometric cues with appearance features. The reliability of geometric structural properties as modality-invariant descriptors is well-established in classical remote sensing matching tasks, such as the Histogram of Oriented Phase Congruency (HOPC) [24], which leverages local geometric structures to bridge the radiometric gap between optical and SAR imagery. Similarly, Xu *et al.* [25] demonstrate that incorporating geometric information can effectively reduce modality discrepancy when appropriately fused with learned representations. Building upon these insights, SDF-Net emphasizes modality-invariant geometric signatures as the core structural anchor while maintaining complementary modality-specific information through an additive residual fusion strategy. This approach achieves a balanced trade-off between robustness to non-linear radiometric distortions and the preservation of discriminative ship identity details.

### C. Optical–SAR Image Analysis and Ship ReID

The development of cross-modal ship re-identification has historically been constrained by the scarcity of standardized benchmarks and large-scale annotated datasets. The recent introduction of the CMShipReID dataset [26] has facilitated ship retrieval across visible, near-infrared, and thermal infrared modalities. However, these sensing modalities are predominantly passive and do not reflect the pronounced modality discrepancy introduced by active microwave imaging. The release of the HOSS-ReID dataset [3] addresses this limitation by providing a dedicated benchmark for optical–SAR association under diverse scattering conditions and complex maritime environments.

Early efforts in bridging the passive-active sensing gap primarily focused on patch-level matching utilizing pseudo-Siamese networks [27]. Transitioning from generic patch

association to instance-level ship retrieval, existing optical–SAR ReID approaches generally fall into three methodological paradigms.

The first paradigm relies on implicit attention-based alignment mechanisms. Representative methods such as TransOSS [3] employ Vision Transformer architectures with specialized tokenization strategies to model global contextual dependencies across modalities. In these approaches, cross-modal correspondence is expected to emerge implicitly from self-attention modeling. However, relying solely on unconstrained self-attention renders the network highly susceptible to modality-specific distractors. Without a definitive physical anchor, the attention mechanism is frequently misled by the discrete, extremely high-intensity corner reflectors in SAR imagery, or complex hydrodynamic wakes in optical data, leading to severe alignment failures. The proposed SDF-Net addresses this critical bottleneck by enforcing a structural consistency constraint, establishing a reliable geometric anchor that prevents the self-attention manifold from collapsing into modality-specific radiometric noise.

The second paradigm focuses on statistical or generative alignment strategies. Inspired by cross-domain adaptation and image translation techniques, these methods attempt to reduce cross-modal distribution divergence through feature-level matching [28] or adversarial image translation frameworks such as CycleGAN [10]. While such approaches can alleviate global modality gaps, they primarily operate at the distribution level and may introduce artificial artifacts or overlook physically grounded structural invariants that remain stable across sensing mechanisms.

The third paradigm incorporates geometry- or physics-guided structural priors into representation learning. In classical optical–SAR matching literature, structural descriptors such as HOPC [24] have demonstrated the effectiveness of leveraging modality-invariant geometric cues to bridge radiometric disparities. Similarly, remote sensing studies have emphasized that structural characteristics are more reliable than raw intensity patterns when associating optical and SAR imagery [2].

Unlike attention-based approaches that implicitly expect geometric correspondence to emerge from global context modeling, or generative methods that attempt to reduce statistical divergence at the distribution level, the proposed SDF-Net encodes structural invariance as a core learning objective. This design grounds cross-modal alignment in physically meaningful geometric primitives rather than relying solely on representation-level similarity. By anchoring identity learning in modality-invariant structural priors and integrating modality-specific cues through residual refinement, the proposed framework establishes a physics-informed representation space. Such a physics-guided, structure-aware formulation remains largely underexplored in optical–SAR ship ReID.

### III. METHODOLOGY

#### A. Problem Definition and Formulation

The objective of optical–SAR ship re-identification is to establish a robust associative mapping between heterogeneous

sensing manifolds. Formally, we define a training dataset as  $\mathcal{D} = \{(I_k, y_k, m_k)\}_{k=1}^N$ , where  $I_k \in \mathbb{R}^{H \times W \times 3}$  denotes the  $k$ -th input image,  $y_k \in \{1, \dots, K\}$  represents the ground-truth identity label from a gallery of  $K$  distinct ships, and  $m_k \in \{0, 1\}$  serves as the modality indicator, with 0 and 1 signifying optical and SAR domains, respectively.

Unlike single-modality retrieval, cross-modal ship ReID requires the network to transcend the massive radiometric gap while preserving identity-critical geometric signatures. We aim to learn a nonlinear mapping function  $\Phi : I \rightarrow \mathbf{f}$  that projects raw pixels into a unified, modality-invariant latent embedding space  $\mathbb{R}^d$ . In this optimized manifold, the learned representations must adhere to a dual constraint: minimizing intra-class variance to facilitate cross-modal identity matching while maximizing inter-class separation to ensure high-fidelity discriminative precision across complex maritime backgrounds.

#### B. Architectural Overview

As illustrated in Fig. 2, the proposed **SDF-Net** is architected upon a Vision Transformer backbone, chosen for its superior capacity to model the global contextual dependencies essential for capturing the elongated structural properties of maritime targets. The input image  $I$  is initially partitioned into  $N_p = (H \times W)/P^2$  non-overlapping patches with a patch stride  $P = 16$ , which are subsequently linearly projected into a sequence of latent tokens.

The network processes these tokens through  $L$  consecutive Transformer blocks to extract hierarchical features. Let  $\mathbf{F}^{(B_s)} \in \mathbb{R}^{B \times C \times H' \times W'}$  denote the feature map derived from the  $B_s$ -th block. To mitigate the profound modality discrepancy induced by active microwave scattering and passive optical reflectance, SDF-Net departs from purely data-driven black-box alignment. Instead, it introduces two physics-guided components:

- **Structure-Aware Consistency Learning (SCL):** This module is strategically embedded at intermediate feature layers to anchor the network on stable geometric skeletons, effectively decoupling the ship’s rigid hull structure from sensor-specific textural fluctuations.
- **Disentangled Feature Learning (DFL):** Operating at the terminal identity stage, this component factorizes the latent representation into a shared identity subspace and a modality-specific auxiliary subspace, employing an additive residual refinement strategy to integrate complementary cues.

#### C. Cross-Modal Feature Tokenization

As illustrated in Fig. 2(a), to accommodate the disparate radiometric properties of optical and SAR sensors, SDF-Net employs a Cross-modal Dual-head Tokenizer at the input stage. Rather than utilizing a generic patch embedding layer, this specialized tokenizer facilitates a modality-aware projection that acknowledges the unique statistical distributions of each sensor. Specifically, the optical and SAR images are processed via independent linear projection heads, which map

## Structure-Aware Disentangled Feature Learning Network (SDF-Net)

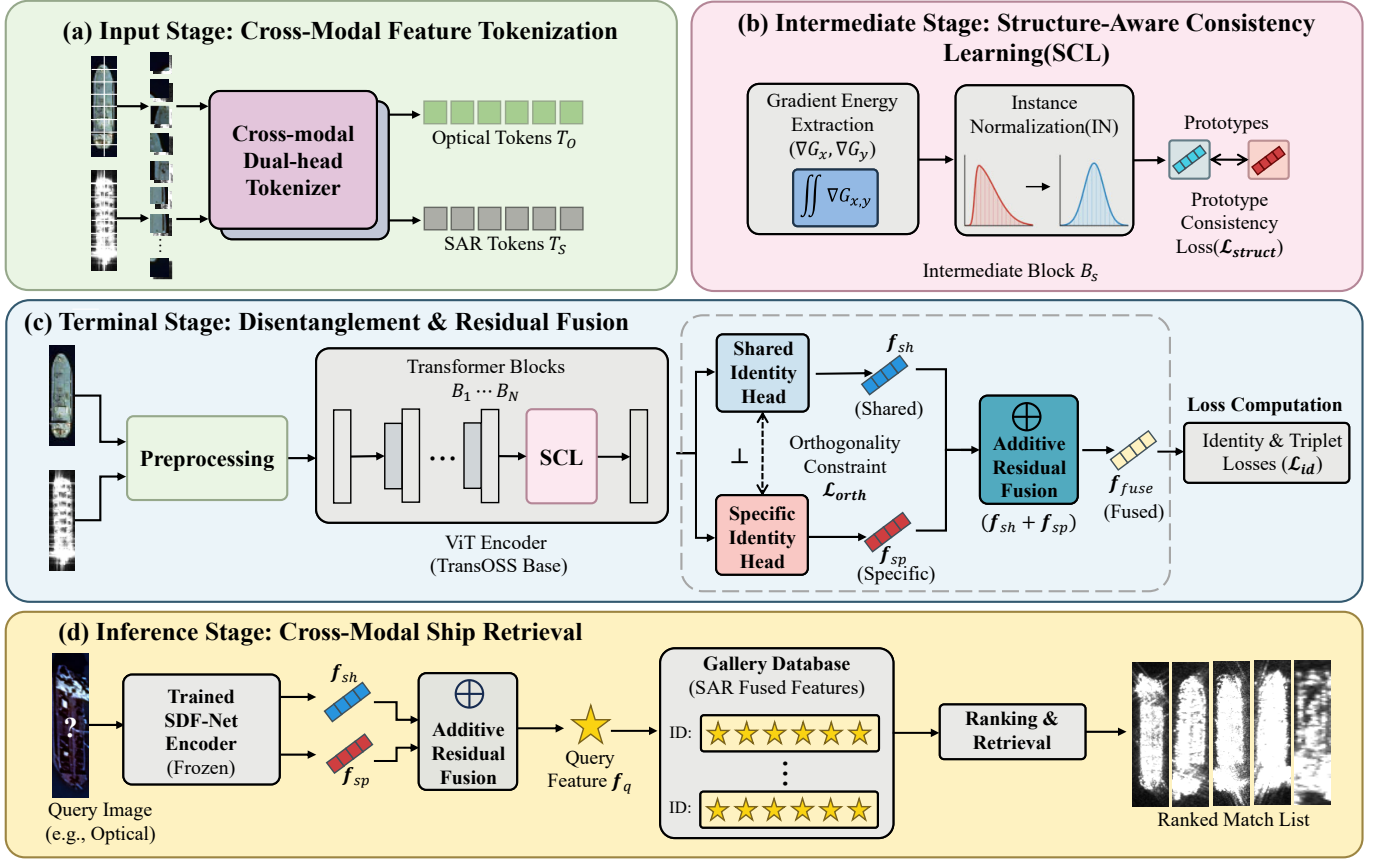


Fig. 2. **Architectural pipeline of the proposed SDF-Net.** The framework is logically structured into four sequential stages: (a) **Input Stage:** Optical and SAR images undergo a cross-modal tokenization strategy to neutralize low-level sensor discrepancies. (b) **Intermediate Stage:** Geometric stability is enforced via the Structure-Aware Consistency Learning (SCL) module, which extracts and aligns intermediate gradient energy to anchor representations on modality-invariant structural primitives. (c) **Terminal Stage:** The final representations are refined by the Disentangled Feature Learning (DFL) module, explicitly decoupling shared identity embeddings from sensor-specific variations before integrating them through an additive residual fusion. (d) **Inference Stage:** The frozen network leverages the robust fused representations to execute accurate bidirectional cross-modal ship retrieval.

the local  $P \times P$  patches into a unified  $C$ -dimensional latent space.

This dual-head configuration is essential for neutralizing low-level sensor discrepancies before the sequences enter the shared Transformer backbone. In the optical domain, the tokenizer primarily captures reflectance-based textural primitives, whereas in the SAR domain, it is tasked with embedding backscatter intensity patterns that are often corrupted by coherent speckle noise. By decoupling the initial tokenization process, the network ensures that the subsequent shared blocks operate on features that have already undergone a coarse radiometric alignment. This preliminary transformation prevents the shared self-attention mechanisms from being dominated by modality-specific intensity biases, thereby allowing the backbone to focus on extracting high-level semantic and geometric invariants.

### D. Structure-Aware Consistency Learning (SCL)

1) *Intermediate Latent Geometry Excavation:* As depicted in Fig. 2(b), a fundamental premise of SDF-Net is that geometric stability is non-uniformly distributed across network layers.

While low-level pixels are excessively corrupted by coherent speckle noise in SAR imagery, and high-level semantic tokens are often too abstract for fine-grained geometric matching, intermediate feature maps act as a critical juncture. These layers retain sufficient spatial topology to characterize the ship's physical layout while being sufficiently abstracted from raw radiometric noise.

Unlike traditional hand-crafted structural descriptors (e.g., HOG or HOPC) that operate directly at the raw pixel level, our approach extracts structural priors from the intermediate latent space. Raw pixel-level gradients are highly susceptible to coherent speckle noise in SAR imagery and high-frequency sea clutter in optical data, inevitably generating severe pseudo-edge artifacts. Conversely, representations at the terminal layers suffer from spatial collapse due to global semantic aggregation. By anchoring our structural probe on the intermediate Transformer feature map  $\mathbf{F}^{(B_s)}$ , SDF-Net elegantly circumvents both extremes. The preceding self-attention blocks effectively filter out low-level radiometric noise, providing a clean, noise-resilient spatial topology where the true rigid hull contours dominate the gradient field.

To characterize geometric structure independent of

modality-specific radiometric responses, we exploit spatial gradient information. For rigid objects such as ships, structural primitives are primarily reflected in spatial intensity variations rather than absolute amplitudes. Gradient operators therefore provide a modality-agnostic descriptor of structural transitions, acting as a high-pass filter that is inherently less sensitive to the multiplicative intensity scaling characteristic of SAR backscatter. For a given intermediate feature map  $\mathbf{F} = \mathbf{F}^{(B_s)}$ , the first-order partial derivatives are computed via index-shifting to capture bidirectional structural variances:

$$\begin{aligned} \mathbf{G}_x(h, w) &= \mathbf{F}(h, w + 1) - \mathbf{F}(h, w - 1), \\ \mathbf{G}_y(h, w) &= \mathbf{F}(h + 1, w) - \mathbf{F}(h - 1, w), \end{aligned} \quad (1)$$

where  $\mathbf{G}_x$  and  $\mathbf{G}_y$  characterize the horizontal and vertical gradient fields, respectively.

To derive a holistic structural representation that is robust to local pixel perturbations, we perform a discrete spatial integration (denoted by the  $\iint \nabla \mathbf{G}_{x,y}$  operator in Fig. 2). By aggregating the absolute gradient magnitudes across the spatial grid, we obtain the structural descriptors:

$$\begin{aligned} \mathbf{e}_x &= \frac{1}{H'W'} \sum_{h,w} |\mathbf{G}_x(h, w)|, \\ \mathbf{e}_y &= \frac{1}{H'W'} \sum_{h,w} |\mathbf{G}_y(h, w)|. \end{aligned} \quad (2)$$

Specifically, given the intermediate feature map  $\mathbf{F}^{(B_s)} \in \mathbb{R}^{B \times C \times H' \times W'}$ , this spatial integration effectively collapses the spatial dimensions, yielding the gradient energy descriptors  $\mathbf{e}_x, \mathbf{e}_y \in \mathbb{R}^{B \times C}$  that summarize the global structural intensity per channel. Crucially, this holistic spatial aggregation mechanism effectively mitigates the adverse impact of isolated high-intensity corner reflectors (strong scattering points) typical in SAR imagery. Instead of being dominated by discrete, localized peaks that could severely corrupt pixel-to-pixel matching, the aggregated gradient energy captures the macroscopic structural contour of the ship. The resulting integrated descriptor  $\mathbf{f}_{\text{struct}} = \mathbf{e}_x + \mathbf{e}_y \in \mathbb{R}^{B \times C}$  serves as a distortion-tolerant, physics-grounded structural anchor. To further neutralize the absolute amplitude disparities between SAR backscatter and optical reflectance,  $\mathbf{f}_{\text{struct}}$  undergoes Instance Normalization (IN) applied independently across the channel dimension  $C$  for each sample.

2) *Scale-Invariant Instance Normalization*: The absolute magnitudes of  $\mathbf{f}_{\text{struct}}$  remain inherently inconsistent across sensors due to the fundamental divergence in imaging physics. SAR images typically exhibit a high dynamic range and skewed energy distributions due to the corner reflector effects of metallic ship hulls, whereas optical images are governed by diffuse reflectance. To achieve radiometric robustness, we apply Instance Normalization (IN) to the descriptors. This operation functions as a statistical filter that maps the disparate energy distributions into a standardized, unit-variance manifold:

$$\hat{\mathbf{f}}_{\text{struct}}^{(b)} = \frac{\mathbf{f}_{\text{struct}}^{(b)} - \mu^{(b)}}{\sqrt{(\sigma^{(b)})^2 + \epsilon}}, \quad (3)$$

where  $\mu^{(b)}$  and  $\sigma^{(b)}$  are the mean and standard deviation computed over the channel dimension  $C$ . This normalization

effectively strips away modality-specific “styles”—such as amplitude bias and illumination variance—while preserving the essential geometric “content” necessary for cross-modal association.

3) *Prototype-level Consistency Loss*: To enforce cross-modal coherence, we align the structural descriptors at a stable identity level rather than at an instance level to avoid overfitting to individual sample noise. For each identity  $i$  in a mini-batch, we define the modality-specific structural prototypes  $\mathbf{c}_i^o$  (optical) and  $\mathbf{c}_i^s$  (SAR):

$$\mathbf{c}_i^o = \frac{1}{|\mathcal{B}_i^o|} \sum_{b \in \mathcal{B}_i^o} \hat{\mathbf{f}}_{\text{struct}}^{(b)}, \quad \mathbf{c}_i^s = \frac{1}{|\mathcal{B}_i^s|} \sum_{b \in \mathcal{B}_i^s} \hat{\mathbf{f}}_{\text{struct}}^{(b)}, \quad (4)$$

where  $\mathcal{B}_i^o$  and  $\mathcal{B}_i^s$  represent the sets of samples for identity  $i$  in each modality. The Structure Consistency Loss  $\mathcal{L}_{\text{struct}}$  minimizes the Euclidean distance between these prototypes:

$$\mathcal{L}_{\text{struct}} = \frac{1}{|\mathcal{I}|} \sum_{i \in \mathcal{I}} \|\mathbf{c}_i^o - \mathbf{c}_i^s\|_2^2. \quad (5)$$

This loss imposes a strong geometric prior on the network, forcing it to prioritize modality-invariant geometric signatures over transient and unreliable textural features.

In practice, the intermediate feature map is extracted from the  $B_s$ -th Transformer block. We empirically select  $B_s = 6$  for a 12-layer backbone, as this layer balances spatial detail preservation and semantic abstraction. Earlier layers tend to be dominated by low-level noise (especially SAR speckle), while deeper layers become overly identity-focused and lose fine-grained structural information. Ablation experiments in Sec. IV further validate the robustness of this choice.

### E. Disentangled Feature Learning and Residual Fusion

As shown in Fig. 2(c), at the terminal stage, the abstract representation  $\mathbf{F}^{(L)} \in \mathbb{R}^{B \times d}$  is fed into two independent linear projection heads, implemented as fully-connected layers without non-linear activations. These parallel branches factorize the terminal representation into the shared identity subspace  $\mathbf{f}_{\text{sh}} \in \mathbb{R}^{B \times d}$  and the modality-specific subspace  $\mathbf{f}_{\text{sp}} \in \mathbb{R}^{B \times d}$ . By maintaining the identical dimensionality  $d$  for both subspaces, we facilitate the subsequent element-wise additive residual fusion without requiring additional channel-matching convolutions. Inspired by the success of orthogonal subspace projection in optimizing deep representation learning [29], we impose an Orthogonality Constraint to ensure the mathematical independence of these feature subspaces:

$$\mathcal{L}_{\text{orth}} = \mathbb{E} \left[ \left\| \left[ \bar{\mathbf{f}}_{\text{sh}}, \bar{\mathbf{f}}_{\text{sp}} \right] \right\| \right], \quad (6)$$

where  $\bar{\mathbf{f}}$  denotes  $\ell_2$ -normalized features. By mathematically minimizing the mutual information between these subspaces, the network is forced to rigorously isolate sensor-independent identity cues in  $\mathbf{f}_{\text{sh}}$ , effectively preventing modality-unique textural nuances from contaminating the invariant geometric anchor.

Rather than discarding  $\mathbf{f}_{\text{sp}}$  as noise, we integrate these features via an additive complementarity strategy:

$$\mathbf{f}_{\text{fuse}} = \mathbf{f}_{\text{sh}} + \mathbf{f}_{\text{sp}}. \quad (7)$$

Physically, this element-wise addition operates as a robust residual refinement mechanism. Since the shared feature  $\mathbf{f}_{sh}$  is strictly regularized by the geometric consistency loss  $\mathcal{L}_{struct}$  to act as the primary cross-modal anchor, superimposing  $\mathbf{f}_{sp}$  does not destruct its established modality invariance. Instead, the specific feature  $\mathbf{f}_{sp}$  adaptively supplements fine-grained, sensor-dependent identity nuances (e.g., unique superstructure scattering distributions or distinct paint reflectances) that are vital for differentiating highly similar ships, thereby maximizing the ultimate re-identification precision without introducing dimensional redundancy.

#### F. Joint Optimization Objective

The unified loss function for training SDF-Net is defined as:

$$\mathcal{L} = \mathcal{L}_{id} + \lambda_{orth} \mathcal{L}_{orth} + \lambda_{struct} \mathcal{L}_{struct}, \quad (8)$$

where  $\mathcal{L}_{id}$  encompasses the label-smoothed cross-entropy loss and the weighted triplet loss for identity supervision. The hyper-parameters  $\lambda_{orth}$  and  $\lambda_{struct}$  serve to balance the influence of feature disentanglement and structural consistency. Through this joint optimization, SDF-Net achieves a harmonious convergence toward a physics-informed identity space that is both robust to modality shifts and highly discriminative for maritime surveillance.

To provide a clear and holistic perspective of the feature abstraction mechanism, the complete forward processing pipeline of SDF-Net is summarized in Algorithm 1. This algorithmic formulation delineates how an input image progressively evolves through the dual-head tokenizer, intermediate structural extraction, and terminal feature disentanglement to form the final robust representation.

## IV. EXPERIMENTS

### A. Dataset

Evaluations are conducted on the HOSS-ReID benchmark, which serves as the primary publicly available resource specifically curated for the cross-modal association of maritime targets. This dataset provides the requisite complexity to validate the robustness of SDF-Net under extreme radiometric disparities between active and passive sensing manifolds. While contemporary maritime datasets such as CMShipReID focus on the alignment of passive sensors including visible, near-infrared, and thermal infrared modalities, HOSS-ReID facilitates research in the more challenging optical-SAR domain where targets are subjected to coherent speckle noise and radar-specific geometric distortions.

The training partition consists of 1,063 images in total, encompassing 574 optical and 489 SAR instances. Such a distribution facilitates the network in learning latent embeddings that remain stable despite the presence of non-linear radiometric fluctuations and varying maritime environmental conditions. Transitioning to the evaluation phase, the testing set is organized into three distinct retrieval protocols to quantify bidirectional and uni-directional search performance. Specifically, Optical-to-SAR uses optical images as queries to retrieve

### Algorithm 1 Forward Processing Pipeline of SDF-Net

**Require:** Input image  $I$ , modality  $m \in \{\text{optical, SAR}\}$ , layer index  $B_s$ , total layers  $L$ .

**Ensure:** Final discriminative identity representation  $\mathbf{f}_{fuse}$ .

#### 1. Cross-modal Dual-head Tokenization

**if**  $m = \text{optical}$  **then**

$\mathbf{T} \leftarrow \text{Tokenizer}_{opt}(I)$

**else**

$\mathbf{T} \leftarrow \text{Tokenizer}_{sar}(I)$

**end if**

#### 2. Intermediate Feature Extraction

$\mathbf{F}^{(B_s)} \leftarrow \text{TransformerBlocks}_{1 \rightarrow B_s}(\mathbf{T})$

#### 3. Structure-Aware Consistency Learning (SCL)

$\mathbf{G}_x, \mathbf{G}_y \leftarrow \nabla_{x,y} \mathbf{F}^{(B_s)}$

$\hat{\mathbf{f}}_{struct} \leftarrow \iint (|\mathbf{G}_x| + |\mathbf{G}_y|)$

$\hat{\mathbf{f}}_{struct} \leftarrow \text{IN}(\hat{\mathbf{f}}_{struct})$

*/\* Training constraint: Optimize  $\mathcal{L}_{struct}$  across modalities \*/*

#### 4. Terminal Feature Extraction

$\mathbf{F}^{(L)} \leftarrow \text{TransformerBlocks}_{B_s+1 \rightarrow L}(\mathbf{F}^{(B_s)})$

#### 5. Disentangled Feature Learning (DFL)

$\mathbf{f}_{sh}, \mathbf{f}_{sp} \leftarrow \text{Decouple}(\mathbf{F}^{(L)})$

*/\* Training constraint: Optimize  $\mathcal{L}_{orth} = \mathbb{E}[\langle \hat{\mathbf{f}}_{sh}, \hat{\mathbf{f}}_{sp} \rangle]$  \*/*

#### 6. Additive Residual Fusion

$\mathbf{f}_{fuse} \leftarrow \mathbf{f}_{sh} + \mathbf{f}_{sp}$

**return**  $\mathbf{f}_{fuse}$

TABLE I  
DETAILED STATISTICAL DISTRIBUTION OF THE HOSS-REID TESTING SET  
ACROSS DIFFERENT EVALUATION PROTOCOLS.

Protocol	Modality	Query images	Gallery images	Total
All-to-All	Optical	88	403	491
	SAR	88	190	278
	<i>Subtotal</i>	<b>176</b>	<b>593</b>	<b>769</b>
Optical-to-SAR	Optical	65	0	65
	SAR	0	190	190
	<i>Subtotal</i>	<b>65</b>	<b>190</b>	<b>255</b>
SAR-to-Optical	SAR	67	0	67
	Optical	0	403	403
	<i>Subtotal</i>	<b>67</b>	<b>403</b>	<b>470</b>

matching targets from a SAR gallery, simulating the real-world scenario of searching for a visually identified ship within historical radar records. Conversely, SAR-to-Optical performs the reverse, using SAR queries to search an optical gallery, which is critical for identifying targets detected at night or under cloud cover. Finally, the All-to-All protocol combines all queries and gallery images regardless of modality, providing a comprehensive and holistic measure of modality-invariant alignment. The precise statistical breakdown of the query and gallery compositions for each protocol is detailed in Table I.

### B. Evaluation Metrics

To rigorously quantify the cross-modal retrieval performance of SDF-Net, we employ two categories of standardized metrics widely recognized in the re-identification community [7]. The Cumulative Match Characteristic (CMC) is utilized to assess the identity matching capability, where the Rank- $k$

accuracy represents the probability that at least one correctly matched candidate appears within the top- $k$  retrieved results. We specifically report Rank-1, Rank-5, and Rank-10 scores to evaluate the model’s precision across varying retrieval breadths. While Rank-1 reflects the primary identification accuracy, the higher-rank metrics provide insight into the robustness of the learned manifold in preserving identity proximity despite severe radiometric distortions.

Parallel to the ranking accuracy, the mean Average Precision (mAP) serves as a holistic descriptor of the retrieval efficacy by accounting for both precision and recall across the entire gallery. For a given query, the Average Precision (AP) is calculated by integrating the area under the precision–recall curve, formulated as:

$$AP = \frac{\sum_{n=1}^N P(n) \times \text{rel}(n)}{G}, \quad (9)$$

where  $N$  denotes the total number of images in the gallery,  $G$  is the count of ground-truth matches, and  $P(n)$  represents the precision at the  $n$ -th rank. The indicator function  $\text{rel}(n)$  is unity if the  $n$ -th result is a correct match and zero otherwise. The final mAP is derived by averaging the AP values across the entire query set of size  $Q$ :

$$mAP = \frac{\sum_{q=1}^Q AP_q}{Q}. \quad (10)$$

In the context of optical–SAR ship re-identification, mAP is particularly critical as it penalizes the failure to retrieve all instances of a target ship, thereby ensuring that the structural anchors learned by SDF-Net effectively bridge the modality gap for all samples of the same identity. These metrics collectively provide a multidimensional assessment of the model’s ability to maintain high discriminative power within a volatile maritime sensing environment.

### C. Implementation Details

All experiments were conducted on a single NVIDIA RTX 3090 GPU equipped with 24GB of VRAM. The software environment is built upon PyTorch 2.2.2 and CUDA 11.8 for hardware acceleration. We adopt the base variant of the Vision Transformer (ViT-B/16) as our backbone network, initialized with weights pre-trained on optical–SAR paired data provided by the TransOSS framework. The input images are uniformly resized to  $256 \times 128$  pixels. To augment the training data and prevent overfitting, we apply random horizontal flipping (with a probability of 0.5), random cropping with zero padding, and random erasing (with a probability of 0.2).

To guarantee the computability of the cross-modal prototype consistency loss  $\mathcal{L}_{\text{struct}}$  and avoid single-modality batches, we implement a strict cross-modal  $P \times K$  sampling strategy. Specifically, each mini-batch of size 32 is constrained to contain exactly  $P = 8$  distinct ship identities. For every identity, we randomly sample  $K = 4$  instances, strictly ensuring a balanced composition of 2 optical images and 2 SAR images. The network is optimized using the Stochastic Gradient Descent (SGD) optimizer with a weight decay of  $1 \times 10^{-4}$ . The initial base learning rate is set to  $5 \times 10^{-4}$ , which

incorporates a linear warmup strategy in the early stage before smoothly decaying over a total of 100 training epochs. The hyper-parameters for the joint loss optimization are empirically set to  $\lambda_{\text{orth}} = 10.0$  and  $\lambda_{\text{struct}} = 1.0$ , with the intermediate structural features extracted from the  $B_s = 6$  Transformer block.

### D. Comparison with State-of-the-Art Methods

The performance of SDF-Net is evaluated against a diverse set of representative algorithms on the HOSS-ReID benchmark, with the comparative results summarized in Table II. The baseline and state-of-the-art methods are categorized into general vision backbones, single-modality re-identification models, and cross-modal retrieval frameworks to provide a comprehensive assessment of the current landscape in maritime surveillance.

General vision backbones and single-modality re-identification models exhibit a pronounced susceptibility to the severe non-linear radiometric distortions inherent in optical–SAR imagery. Although transformer-based architectures such as DeiT-base and TransReID demonstrate superior feature extraction capabilities compared to earlier convolutional counterparts, their performance remains suboptimal due to the absence of explicit cross-modal alignment mechanisms. For instance, TransReID achieves a modest 20.9% mAP under the SAR-to-Optical protocol, underscoring the inadequacy of standard appearance-based matching when confronted with the coherent speckle noise and geometric artifacts of radar imaging. While these models effectively capture high-level semantics, they fail to bridge the disparate sensing manifolds without specialized constraints.

Existing cross-modal re-identification methods, primarily optimized for visible–infrared person re-identification, similarly struggle to generalize to the maritime domain. Approaches such as DEEN and VersReID are designed to align passive thermal radiation with visible reflectance, a task that does not account for the drastic imaging discrepancies between active microwave backscattering and optical imagery. This domain mismatch is evident in the performance of AMML and CM-NAS, which yield significantly lower accuracies than the remote-sensing-specific baseline. The inability of these models to capture stable geometric invariants leads to substantial alignment failures in the presence of fluctuating sea clutter and varying draft depths.

SDF-Net consistently achieves highly competitive or superior performance over all state-of-the-art methods across every evaluation metric and retrieval protocol. Under the comprehensive All protocol, the proposed method achieves 60.9% mAP and 69.9% Rank-1 accuracy, representing an improvement of 3.5% and 4.0% respectively over the current leading baseline, TransOSS. The performance margin is particularly significant in the SAR-to-Optical task, where SDF-Net elevates the mAP from 38.7% to 46.6%. This 7.9% absolute increase validates the efficacy of anchoring identity representations on modality-invariant geometric skeletons through the Structure-Aware Consistency learning module. By leveraging the rigid hull structure as a definitive physical anchor, SDF-Net maintains a

TABLE II

QUANTITATIVE EVALUATION OF THE PROPOSED SDF-NET COMPARED WITH STATE-OF-THE-ART METHODS ON THE HOSS-REID BENCHMARK. ALL VALUES ARE REPORTED IN PERCENTAGE (%).

Task Type	Method	Venue	All-to-All				Optical-to-SAR				SAR-to-Optical			
			mAP	R1	R5	R10	mAP	R1	R5	R10	mAP	R1	R5	R10
General model	ViT-base [30]	Arxiv2020	43.0	56.2	64.8	69.9	21.5	12.3	33.8	55.4	17.9	10.4	25.4	32.8
	DeiT-base [31]	ICML2021	47.2	58.1	69.6	74.1	25.9	16.1	36.7	59.1	26.1	10.3	35.7	52.0
Single modality ReID	AGW [7]	TPAMI2021	43.6	57.4	64.2	68.8	17.2	7.7	29.2	38.5	21.1	14.9	34.3	46.3
	TransReID [9]	ICCV2021	48.1	60.8	69.3	73.9	27.3	18.5	40.0	58.5	20.9	11.9	34.3	43.3
	SOLIDER [32]	CVPR2023	38.2	50.6	63.1	69.9	23.1	12.3	38.5	52.3	14.6	10.4	16.4	31.3
	D2InterNet [33]	SIGIR2025	50.2	59.1	71.6	79.0	33.0	21.5	41.5	69.8	28.8	25.4	38.8	50.7
Cross-modal ReID	Hc-Tri [34]	TMM2020	34.0	47.2	54.6	59.7	11.1	6.2	15.4	24.6	10.9	7.5	20.9	29.9
	CM-NAS [35]	CVPR2021	30.7	46.0	54.6	57.4	8.2	1.5	10.8	21.5	7.6	4.5	11.9	19.4
	LbA [36]	CVPR2021	33.0	48.3	59.7	62.5	11.9	4.6	23.1	41.5	8.5	6.0	14.9	22.4
	DEEN [37]	CVPR2023	43.8	58.5	64.2	66.5	31.3	21.5	44.6	60.0	27.4	22.4	40.3	53.7
	MCJA [38]	TCSVT2024	47.1	59.1	67.9	73.0	18.6	10.8	27.7	38.5	19.7	14.9	28.3	43.3
	VersReID [39]	TPAMI2024	49.3	59.7	70.5	78.4	25.7	13.8	40.0	61.5	27.7	17.9	44.8	61.2
	AMML [40]	IJCV2025	31.2	43.8	52.8	56.8	9.1	4.6	10.8	21.5	9.2	4.5	13.4	20.9
	HSFLNet [41]	EAAI2025	22.8	29.0	44.9	52.3	19.0	13.9	24.6	32.3	19.2	19.4	26.9	46.3
	TransOSS [3]	ICCV2025	57.4	65.9	79.5	85.8	48.9	33.8	<b>67.7</b>	80.0	38.7	29.9	59.7	71.6
	<b>SDF-Net (ours)</b>	-	-	<b>60.9</b>	<b>69.9</b>	<b>81.8</b>	<b>88.1</b>	<b>50.0</b>	<b>35.4</b>	<b>67.7</b>	<b>86.2</b>	<b>46.6</b>	<b>38.8</b>	<b>70.1</b>

robust shared manifold that is far less sensitive to radiometric fluctuations than the implicit global attention mechanisms utilized in TransOSS. The additive residual fusion strategy further enhances the discriminative precision of the model by integrating modality-specific nuances as refinements rather than noise, establishing a new state-of-the-art for cross-modal maritime target association.

### E. Ablation Studies

The architectural integrity and performance gains of SDF-Net are validated through a systematic dissection across three critical axes. First, we evaluate the fundamental contributions of the Structure-Aware Consistency Learning (SCL) and Disentangled Feature Learning (DFL) modules to establish the necessity of each component. Second, the efficacy of disparate feature integration strategies—comprising summation, shared-only, specific-only, and concatenation—is assessed to determine the optimal fusion paradigm. Finally, we investigate the sensitivity of the geometric extraction layer to identify the block index that most effectively captures modality-invariant structural primitives. All experiments are conducted on the HOSS-ReID dataset following the standard evaluation protocols.

1) *Effectiveness of Proposed Modules:* The individual and synergistic impacts of SCL and DFL are quantified by progressively integrating them into the vanilla backbone. As evidenced by the results in Table III, the isolated inclusion of SCL yields a measurable enhancement in retrieval stability, particularly elevating the SAR-to-Optical mAP from 44.5% to 46.6%. This improvement suggests that enforcing geometric consistency at intermediate layers effectively anchors the representation space against the radiometric fluctuations inherent in SAR imagery. Notably, while the SCL constraint primarily optimizes the structural alignment, the DFL module serves as a decisive driver for discriminative precision. The introduction of DFL significantly boosts the Rank-1 accuracy from 67.6% to 69.9% in the All-to-All setting, confirming that decoupling

modality-specific noise from shared identity cues facilitates a more robust feature manifold.

TABLE III

ABLATION STUDY HIGHLIGHTING THE EFFECTIVENESS OF THE SCL AND DFL MODULES ON THE HOSS-REID BENCHMARK. ALL VALUES ARE REPORTED IN PERCENTAGE (%).

SCL	DFL	All-to-All		Optical-to-SAR		SAR-to-Optical	
		mAP	R1	mAP	R1	mAP	R1
$\times$	$\times$	58.6	67.6	46.5	32.3	44.5	<b>38.8</b>
$\checkmark$	$\times$	59.2	66.5	47.6	32.3	<b>46.6</b>	37.3
$\times$	$\checkmark$	59.8	<b>69.9</b>	49.3	<b>35.4</b>	41.4	31.3
$\checkmark$	$\checkmark$	<b>60.9</b>	<b>69.9</b>	<b>50.0</b>	<b>35.4</b>	<b>46.6</b>	<b>38.8</b>

The full configuration of SDF-Net achieves the most balanced performance, reaching a peak mAP of 60.9% and restoring the optimal Rank-1 accuracy across all protocols. Although SCL applied in isolation occasionally introduces subtle fluctuations in directional Rank-1 metrics due to the stringent geometric regularization, its synergy with DFL is paramount for reconciling rigid hull structures with fine-grained identity refinement. This dual-constraint mechanism ensures that the model moves beyond implicit statistical alignment, establishing a physics-informed representation space that is far more resilient to the non-linear modality gap.

2) *Sensitivity Analysis of Structural Extraction Layer:* To determine the optimal abstraction level for anchoring geometric consistency, we investigate the impact of the insertion depth for the Structure Consistency Constraint by varying the feature extraction layer index  $B_s$  within the Vision Transformer backbone. As presented in Table IV, extracting structural priors from shallow layers such as  $B_s = 2$  yields suboptimal retrieval accuracy. This underperformance is attributed to the prevalence of low-level radiometric noise and coherent speckle artifacts in the early processing stages, which corrupt the gradient energy statistics before sufficient semantic filtering occurs.

Performance metrics improve significantly as the extraction point shifts toward intermediate layers, confirming that mid-level representations effectively retain spatial topology while abstracting away sensor-specific interference. Specifically, the configuration with  $B_s = 6$  attains the peak holistic performance, achieving an mAP of 60.9% and Rank-1 accuracy of 69.9% under the All protocol. Although  $B_s = 4$  exhibits competitive results and slightly higher Optical-to-SAR precision, the  $B_s = 6$  setting demonstrates superior robustness in the more challenging SAR-to-Optical scenario, delivering an mAP of 46.6% compared to 45.3% at  $B_s = 4$ . This indicates that the sixth layer offers a more balanced trade-off between suppressing optical texture variations and preserving radar geometric signatures.

Conversely, enforcing structural consistency at deeper layers leads to a discernible performance degradation. The results at  $B_s = 8$  and  $B_s = 10$  reveal that high-level semantic features become overly abstract and spatially collapsed, thereby losing the fine-grained geometric layout information essential for pixel-wise gradient alignment. Consequently, intermediate layers serve as the most reliable structural probe, motivating the selection of  $B_s = 6$  as the default configuration for SDF-Net.

TABLE IV

ABLATION STUDY ON THE STRUCTURAL EXTRACTION LAYER INDEX  $B_s$ . THE RESULTS INDICATE THAT EXTRACTING STRUCTURAL PRIORS AT INTERMEDIATE LAYERS (E.G.,  $B_s = 6$ ) ACHIEVES THE OPTIMAL TRADE-OFF BETWEEN SPATIAL FIDELITY AND SEMANTIC ABSTRACTION. ALL VALUES ARE REPORTED IN PERCENTAGE (%).

$B_s$	All-to-All		Optical-to-SAR		SAR-to-Optical	
	mAP	R1	mAP	R1	mAP	R1
2	59.7	68.2	49.0	35.4	46.0	<b>40.3</b>
4	60.4	68.8	<b>50.5</b>	<b>38.5</b>	45.3	38.8
<b>6</b>	<b>60.9</b>	<b>69.9</b>	50.0	35.4	<b>46.6</b>	38.8
8	58.4	65.3	48.7	35.4	45.5	<b>40.3</b>
10	58.7	66.5	48.9	33.8	44.7	37.3
12	60.3	<b>69.9</b>	47.4	33.8	45.3	34.3

3) *Evaluation of Feature Fusion Strategies:* To validate the rationale behind the additive complementarity design, we examine the discriminative contribution of the disentangled subspaces and compare different integration mechanisms. As detailed in Table V, utilizing the modality-specific feature  $\mathbf{f}_{sp}$  in isolation yields the lowest performance, with an mAP of 58.7% under the All protocol. This confirms that sensor-dependent characteristics, such as SAR speckle patterns or optical color textures, are insufficient for reliable cross-modal matching when detached from the underlying identity structure.

In contrast, the shared identity feature  $\mathbf{f}_{sh}$  alone achieves a reputable mAP of 59.2%, substantiating the effectiveness of the orthogonality constraint in isolating modality-invariant cues. However, a performance plateau is observed, indicating that discarding all modality-specific information inevitably results in a loss of fine-grained discriminative details.

Integrating these two subspaces leads to further improvements, yet the fusion method proves critical. The concatenation strategy  $\text{Cat}(\mathbf{f}_{sh}, \mathbf{f}_{sp})$  results in an mAP of 59.5% under the All

protocol. Although it slightly edges out the additive strategy in the Optical-to-SAR mAP (50.7%), it introduces a twofold expansion of the feature dimension, imposing unnecessary computational overhead and redundancy on the subsequent retrieval heads. Conversely, the proposed additive fusion  $\mathbf{f}_{sh} + \mathbf{f}_{sp}$  delivers the most comprehensive and robust performance, reaching the peak 60.9% mAP and 69.9% Rank-1 accuracy under the primary All-to-All protocol, while also dominating the more challenging SAR-to-Optical task. This suggests that treating modality-specific features as a parameter-efficient residual refinement to the shared identity embedding effectively maximizes discriminability without expanding the original feature dimensionality.

TABLE V

ABLATION STUDY ON FEATURE FUSION STRATEGIES. THE ADDITIVE INTERACTION ACTS AS A PARAMETER-EFFICIENT RESIDUAL REFINEMENT, OUTPERFORMING CONCATENATION AND SINGLE-BRANCH BASELINES. ALL VALUES ARE REPORTED IN PERCENTAGE (%).

Fusion Strategy	All-to-All		Optical-to-SAR		SAR-to-Optical	
	mAP	R1	mAP	R1	mAP	R1
Specific-only ( $\mathbf{f}_{sp}$ )	58.7	67.6	44.3	29.2	43.9	35.8
Shared-only ( $\mathbf{f}_{sh}$ )	59.2	68.2	49.8	33.8	43.1	37.3
Concatenation	59.5	68.8	<b>50.7</b>	<b>35.4</b>	45.1	35.8
<b>Additive (Ours)</b>	<b>60.9</b>	<b>69.9</b>	50.0	<b>35.4</b>	<b>46.6</b>	<b>38.8</b>

4) *Computational Complexity Analysis:* To validate the efficiency of the proposed framework, we quantify the computational complexity and parameter count of SDF-Net against the leading baseline, TransOSS. As summarized in Table VI, thanks to the parameter-free nature of the spatial gradient integration and instance normalization within the SCL module, alongside the element-wise additive fusion in the DFL module, SDF-Net introduces absolutely zero additional parameters. Specifically, both SDF-Net and the baseline strictly maintain 86.24 M parameters. In terms of computational overhead, SDF-Net requires 22.42 G FLOPs during inference, representing a negligible increase of merely 0.17 G FLOPs compared to the 22.25 G FLOPs of the baseline. This marginal computational addition (less than a 0.8% increase) yields a substantial 3.5% absolute improvement in the comprehensive mAP (from 57.4% to 60.9%) and a 4.0% increase in Rank-1 accuracy (from 65.9% to 69.9%). These statistics conclusively demonstrate that SDF-Net achieves superior physics-guided cross-modal alignment in a highly parameter- and compute-efficient manner, avoiding the prohibitive overhead typical of complex generative or attention-heavy alignment strategies.

TABLE VI

COMPUTATIONAL COMPLEXITY AND PERFORMANCE COMPARISON BETWEEN THE BASELINE AND THE PROPOSED SDF-NET.

Method	Params (M)	FLOPs (G)	mAP (%)	Rank-1 (%)
TransOSS	86.24	22.25	57.4	65.9
<b>SDF-Net</b>	86.24	22.42	60.9	69.9

5) *Hyper-parameter Sensitivity Analysis:* To thoroughly investigate the stability of the proposed framework, we conduct a sensitivity analysis on the two critical hyper-parameters:

the orthogonality weight  $\lambda_{\text{orth}}$  and the structural consistency weight  $\lambda_{\text{struct}}$ . As visualized in the heatmaps in Fig. 3, the model performance exhibits robust tolerance across a wide range of parameter combinations.

The structural weight  $\lambda_{\text{struct}}$  is optimal around 1.0, effectively bridging the modality gap without overwhelmingly dictating the semantic feature space. Concurrently, increasing the orthogonality weight  $\lambda_{\text{orth}}$  progressively forces the disentanglement of shared and specific features, reaching peak discriminative capacity at  $\lambda_{\text{orth}} = 10.0$ . Deviations from these optimal settings lead to gentle performance degradation rather than catastrophic failure, confirming that SDF-Net is not reliant on excessive hyper-parameter tuning and demonstrating strong generalization potential for cross-modal maritime retrieval tasks.

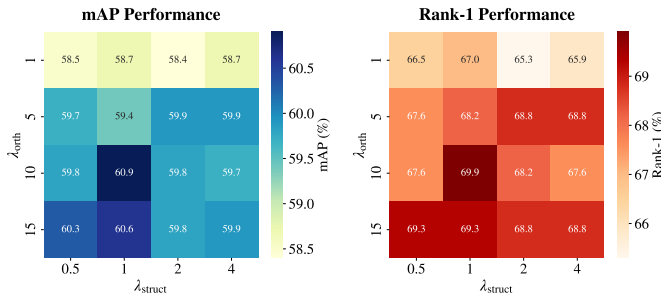


Fig. 3. Hyper-parameter sensitivity analysis of SDF-Net. The heatmaps illustrate the variation of mAP (left) and Rank-1 (right) accuracies (in %) under different combinations of the orthogonality constraint weight  $\lambda_{\text{orth}}$  and the structure consistency weight  $\lambda_{\text{struct}}$ .

#### F. Visualization and Qualitative Analysis

To systematically demystify the internal representation mechanism and evaluate the practical efficacy of SDF-Net, we conduct a comprehensive multi-level qualitative analysis. We first visualize the spatial attention distribution to confirm that the network successfully anchors on modality-invariant structural priors while suppressing sensor-specific interference. Building upon this, we trace the evolutionary trajectory of intermediate feature maps to physically interpret the process of geometric abstraction and justify our architectural design choices. Finally, these theoretical insights are projected into the practical application domain by contrasting the ultimate retrieval results against the baseline, conclusively demonstrating the robustness of the proposed framework in bridging the complex optical–SAR modality gap.

1) *Class Activation Mapping Analysis*: To qualitatively validate the representation alignment mechanism of the proposed framework, we employ Grad-CAM to visualize the spatial attention distributions across heterogeneous sensing modalities. As illustrated in Fig. 4, SDF-Net yields highly concentrated and geometrically consistent activation responses across both the passive reflectance and active backscatter manifolds. Driven by the Structure-Aware Consistency learning module, the network consistently anchors its attention on the rigid hull contours and spatial layout of the maritime targets regardless of the imaging mechanism.

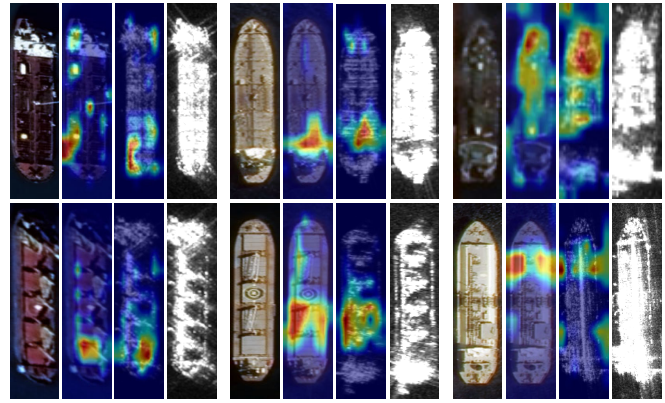


Fig. 4. Grad-CAM visualization of the spatial attention maps generated by SDF-Net. From left to right within each group: the input optical image, the corresponding optical attention map, the SAR attention map, and the input SAR image. The network consistently focuses on the modality-invariant ship hull structure, effectively suppressing optical sea clutter and penetrating SAR speckle noise.

Specifically, within the optical domain, the network’s attention successfully localizes the primary discriminative regions of the ships while effectively mitigating the influence of surrounding sea clutter. Crucially, the corresponding SAR activations exhibit a highly consistent spatial distribution. Despite the severe interference from inherent coherent speckle noise and high-intensity scattering artifacts, the model reliably attends to the corresponding spatial locations of the target. This strict cross-modal attention coherence substantiates the premise that enforcing intermediate structural constraints encourages the network to anchor its feature representations on modality-invariant spatial layouts rather than sensor-dependent textures, thereby establishing a robust identity association.

2) *Visual Analysis of Layer-wise Feature Evolution*: To elucidate the underlying mechanism of the Structure-Aware Consistency learning module, we examine the evolutionary trajectory of spatial representations by extracting feature heatmaps from varying depths of the Vision Transformer backbone. As presented in Fig. 5, the progression from shallow to deep layers reveals a distinct transition spanning from low-level sensor interference to high-level semantic abstraction.

In the early processing stages, specifically at layers 2 and 4, the feature maps exhibit high spatial resolution but remain severely entangled with modality-specific artifacts. Within the optical domain, the attention responses are heavily distracted by local background variations and illumination inconsistencies. Concurrently, the corresponding SAR features are dominated by discrete, high-intensity backscattering points and coherent speckle noise. This confirms that shallow token representations retain excessive sensor-dependent characteristics, rendering them unsuitable for direct geometric alignment.

As the hierarchical extraction progresses to the intermediate phase at layer 6, a profound spatial refinement occurs. The network effectively filters out the modality-specific radiometric distortions, distilling a concentrated and clean spatial layout of the ship. The physical proportions and topological structures are robustly preserved at this specific depth, providing an optimal and stable structural anchor for cross-modal match-

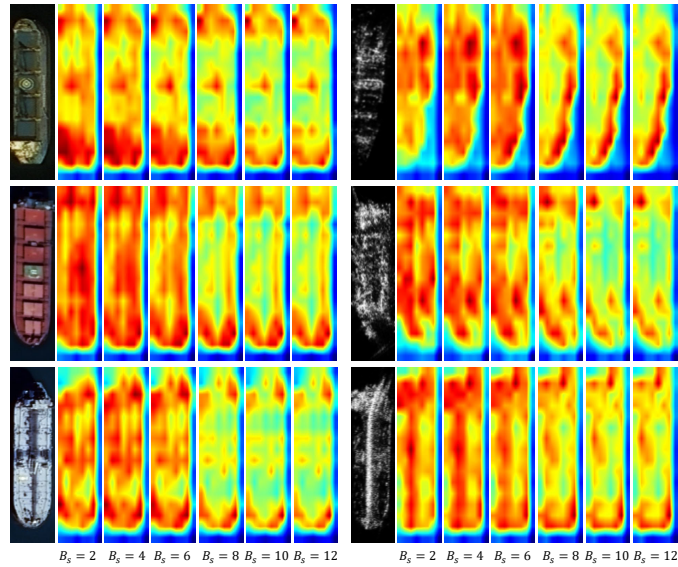


Fig. 5. Visual evolution of feature heatmaps across different Transformer layers. For each modality group, the columns from left to right represent the original input image followed by the feature activation maps extracted from layers 2, 4, 6, 8, 10, and 12. Intermediate representations at layer 6 successfully isolate the modality-invariant geometric structure, whereas shallow layers are corrupted by sensor noise and deep layers suffer from spatial semantic collapse.

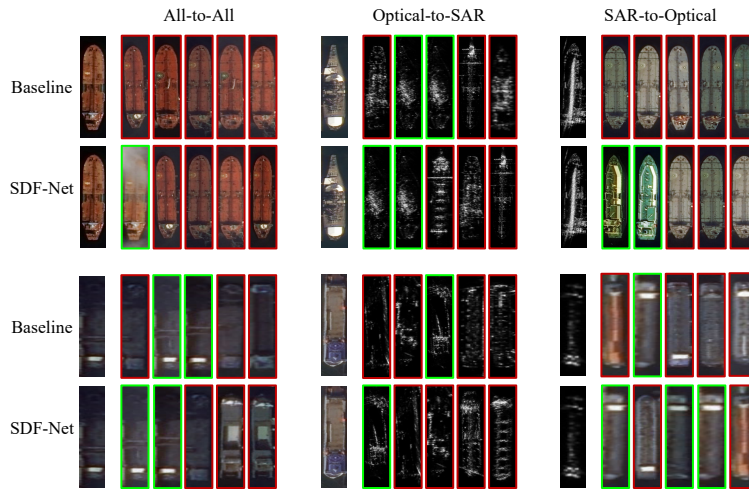


Fig. 6. Qualitative comparison of retrieval results between the baseline and the proposed SDF-Net across three evaluation protocols. The left, middle, and right columns correspond to the All-to-All, Optical-to-SAR, and SAR-to-Optical settings, respectively. Green bounding boxes indicate correct matches, while red bounding boxes represent incorrect matches. SDF-Net exhibits superior robustness against modality-specific noise, consistently retrieving correct physical identities at higher ranks compared to the appearance-biased baseline.

ing. This visual phenomenon directly corroborates our prior quantitative ablation findings, which identify the sixth block as the optimal insertion point for the structural consistency constraint.

Conversely, the visualizations derived from the deeper stages spanning layers 8 through 12 demonstrate a progressive degradation of spatial fidelity. Driven by the terminal identity classification objective, the deep self-attention mechanisms aggressively aggregate global context. Consequently, the feature responses become spatially collapsed and overly abstract. Although these terminal representations encapsulate the highly discriminative semantic cues necessary for the final retrieval, they largely lose the fine-grained physical localization required for explicit structural regularization.

3) *Qualitative Retrieval Comparison:* To intuitively demonstrate the superiority of the proposed framework in bridging the heterogeneous sensing gap, we visualize the top-ranked retrieval results of SDF-Net alongside the baseline model. As illustrated in Fig. 6, the qualitative evaluation is conducted across the All, Optical-to-SAR, and SAR-to-Optical protocols.

The baseline model exhibits a pronounced vulnerability to the non-linear radiometric distortions inherent in cross-modal matching. Driven primarily by global appearance and texture similarities, the baseline frequently retrieves false positive candidates—indicated by red bounding boxes—at the highest ranks. This failure mechanism is particularly evident in the highly challenging Optical-to-SAR and SAR-to-Optical

scenarios. Instead of matching the physical identity of the ships, the baseline tends to associate queries with gallery images sharing analogous maritime backgrounds, similar draft patterns, or comparable coherent speckle noise distributions. Such behavior underscores the fragility of purely statistical alignment when lacking explicit physical constraints.

Conversely, SDF-Net consistently identifies the correct targets, achieving a significantly higher density of true positive matches, denoted by green bounding boxes, across all evaluated ranks and protocols. By anchoring the feature representation on modality-invariant geometric skeletons through the Structure-Aware Consistency learning module, the proposed network successfully circumvents the interference of complex sea clutter and radar artifacts. Even when querying with low-resolution SAR images highly corrupted by speckle noise, SDF-Net accurately retrieves the corresponding optical counterparts based on invariant structural primitives such as hull contours and spatial layouts. This robust qualitative performance directly corroborates the substantial quantitative margins observed in the primary evaluation metrics, conclusively validating the efficacy of physics-guided disentangled learning for maritime target association.

## V. CONCLUSION

This paper introduces SDF-Net, a physics-guided representation learning framework designed to tackle the severe non-linear radiometric disparities in optical-SAR ship re-identification. Moving beyond conventional appearance-based matching, SDF-Net firmly anchors cross-modal association on modality-invariant geometric structures. Specifically, the Structure-Aware Consistency Learning (SCL) module extracts intermediate gradient energy to isolate the rigid ship hull from sensor-specific interference. Furthermore, the Disentangled Feature Learning (DFL) component factorizes terminal representations into shared identity and modality-specific subspaces, integrating them via a parameter-efficient additive fusion to preserve fine-grained discriminative nuances without dimensional redundancy. Extensive evaluations on the HOSS-ReID benchmark conclusively demonstrate that SDF-Net achieves state-of-the-art performance, exhibiting profound robustness against complex sea clutter and radar artifacts. However, reliance on gradient energy may encounter limitations when querying extremely low-resolution SAR targets whose structural contours are entirely submerged in dense speckle noise. Furthermore, while the current framework is predicated on overhead or near-vertical observation perspectives, real-world satellite imagery often contains severe 3D structural distortions caused by extreme and varying incidence angles. Acknowledging these physical boundary conditions, future research will focus on extending this structure-centric alignment paradigm to handle multi-view geometric distortions, and exploring unsupervised geometric distillation to further bridge the physical gap between highly heterogeneous remote sensing modalities.

## VI. ACKNOWLEDGMENT

The authors would like to thank all the researchers who kindly shared the codes.

## REFERENCES

- [1] G. Fracastoro, E. Magli, G. Poggi, G. Scarpa, D. Valsesia, and L. Verdoliva, "Deep learning methods for synthetic aperture radar image despeckling: An overview of trends and perspectives," *IEEE Geoscience and Remote Sensing Magazine*, vol. 9, no. 2, pp. 29–51, 2021. 1
- [2] M. Schmitt, L. H. Hughes, C. Qiu, and X. X. Zhu, "Sen12ms – a curated dataset of georeferenced multi-spectral sentinel-1/2 imagery for deep learning and data fusion," *ISPRS Annals of the Photogrammetry, Remote Sensing and Spatial Information Sciences*, vol. IV-2/W7, pp. 153–160, 2019. 1, 2, 3, 4
- [3] H. Wang, S. Li, J. Yang, Y. Liu, Y. Lv, and Z. Zhou, "Cross-modal ship re-identification via optical and sar imagery: A novel dataset and method," in *Proceedings of the IEEE/CVF International Conference on Computer Vision (ICCV)*, October 2025, pp. 7873–7883. 1, 2, 3, 4, 9
- [4] L. H. Hughes, M. Schmitt, L. Mou, Y. Wang, and X. X. Zhu, "Identifying corresponding patches in sar and optical images with a pseudo-siamese cnn," *IEEE Geoscience and Remote Sensing Letters*, vol. 15, no. 5, pp. 784–788, 2018. 1
- [5] N. Merkle, S. Auer, R. Mueller, and P. Reinartz, "Exploring the potential of conditional adversarial networks for optical and sar image matching," *IEEE Journal of Selected Topics in Applied Earth Observations and Remote Sensing*, vol. 11, no. 6, pp. 1811–1820, 2018. 1
- [6] T. Zhang, X. Zhang, X. Ke, X. Zhan, J. Shi, S. Wei, D. Pan, J. Li, H. Su, Y. Zhou *et al.*, "Ls-ssdd-v1. 0: A deep learning dataset dedicated to small ship detection from large-scale sentinel-1 sar images," *Remote Sensing*, vol. 12, no. 18, p. 2997, 2020. 1
- [7] M. Ye, J. Shen, G. Lin, T. Xiang, L. Shao, and S. C. H. Hoi, "Deep learning for person re-identification: A survey and outlook," *IEEE Transactions on Pattern Analysis and Machine Intelligence*, 2021. 1, 2, 7, 9
- [8] J. Liu, Y. Sun, F. Zhu, H. Pei, Y. Yang, and W. Li, "Learning memory-augmented unidirectional metrics for cross-modality person re-identification," in *Proceedings of the IEEE/CVF Conference on Computer Vision and Pattern Recognition (CVPR)*, June 2022, pp. 19 366–19 375. 1
- [9] S. He, H. Luo, P. Wang, F. Wang, H. Li, and W. Jiang, "Transreid: Transformer-based object re-identification," in *Proceedings of the IEEE/CVF international conference on computer vision*, 2021, pp. 15 013–15 022. 1, 9
- [10] J.-Y. Zhu, T. Park, P. Isola, and A. A. Efros, "Unpaired image-to-image translation using cycle-consistent adversarial networks," in *Proceedings of the IEEE international conference on computer vision*, 2017, pp. 2223–2232. 2, 4
- [11] L. Li, M. Liu, L. Ma, and L. Han, "Cross-modal feature description for remote sensing image matching," *International Journal of Applied Earth Observation and Geoinformation*, vol. 112, p. 102964, 2022. 2
- [12] X. Yang, J. Zhao, Z. Wei, N. Wang, and X. Gao, "Sar-to-optical image translation based on improved cgan," *Pattern Recognition*, vol. 121, p. 108208, 2022. 2
- [13] Z. Zheng, X. Yang, Z. Yu, L. Zheng, Y. Yang, and J. Kautz, "Joint discriminative and generative learning for person re-identification," in *proceedings of the IEEE/CVF conference on computer vision and pattern recognition*, 2019, pp. 2138–2147. 2, 3
- [14] K. Ren and L. Zhang, "Implicit discriminative knowledge learning for visible-infrared person re-identification," in *Proceedings of the IEEE/CVF Conference on Computer Vision and Pattern Recognition (CVPR)*, June 2024, pp. 393–402. 2
- [15] X. Fang, Y. Yang, and Y. Fu, "Visible-infrared person re-identification via semantic alignment and affinity inference," in *Proceedings of the IEEE/CVF International Conference on Computer Vision (ICCV)*, October 2023, pp. 11 270–11 279. 2
- [16] S. Zhang, Y. Yang, P. Wang, G. Liang, X. Zhang, and Y. Zhang, "Attend to the difference: Cross-modality person re-identification via contrastive correlation," *IEEE Transactions on Image Processing*, vol. 30, pp. 8861–8872, 2021. 2
- [17] C. Chen, M. Ye, M. Qi, J. Wu, J. Jiang, and C.-W. Lin, "Structure-aware positional transformer for visible-infrared person re-identification," *IEEE Transactions on Image Processing*, vol. 31, pp. 2352–2364, 2022. 3
- [18] H. Zheng, X. Zhong, W. Huang, K. Jiang, W. Liu, and Z. Wang, "Visible-infrared person re-identification: A comprehensive survey and a new setting," *Electronics*, vol. 11, no. 3, p. 454, 2022. 3
- [19] X. Zhang, Z. Huang, X. Yao, X. Feng, G. Cheng, and J. Han, "Cross-modality domain adaptation based on semantic graph learning: From optical to sar images," *IEEE Transactions on Geoscience and Remote Sensing*, 2025. 3

- [20] S. Choi, S. Lee, Y. Kim, T. Kim, and C. Kim, "Hi-cmd: Hierarchical cross-modality disentanglement for visible-infrared person re-identification," in *Proceedings of the IEEE/CVF conference on computer vision and pattern recognition*, 2020, pp. 10 257–10 266. 3
- [21] X. Pan, P. Luo, J. Shi, and X. Tang, "Two at once: Enhancing learning and generalization capacities via ibn-net," in *Proceedings of the european conference on computer vision (ECCV)*, 2018, pp. 464–479. 3
- [22] L. A. Gatys, A. S. Ecker, and M. Bethge, "Image style transfer using convolutional neural networks," in *Proceedings of the IEEE conference on computer vision and pattern recognition*, 2016, pp. 2414–2423. 3
- [23] R. Zhang, P. Isola, A. A. Efros, E. Shechtman, and O. Wang, "The unreasonable effectiveness of deep features as a perceptual metric," in *Proceedings of the IEEE conference on computer vision and pattern recognition*, 2018, pp. 586–595. 3
- [24] Y. Ye and L. Shen, "Hopc: A novel similarity metric based on geometric structural properties for multi-modal remote sensing image matching," *ISPRS Annals of the Photogrammetry, Remote Sensing and Spatial Information Sciences*, vol. III-1, pp. 9–16, 2016. 3, 4
- [25] Q. Xu and X. Zhao, "Contour-guided modality mitigation network for visible-infrared person re-identification," in *2024 IEEE International Conference on Multimedia and Expo (ICME)*, 2024, pp. 1–6. 3
- [26] C. Xu, L. Gao, Y. Liu, Q. Zhang, N. Su, S. Zhang, T. Li, and X. Zheng, "Cmshipreid: A cross-modality ship dataset for the re-identification task," *IEEE Journal of Selected Topics in Applied Earth Observations and Remote Sensing*, 2025. 3
- [27] L. H. Hughes, M. Schmitt, L. Mou, Y. Wang, and X. X. Zhu, "Identifying corresponding patches in sar and optical images with a pseudo-siamese cnn," *IEEE Geoscience and Remote Sensing Letters*, vol. 15, no. 5, pp. 784–788, 2018. 3
- [28] M. Long, Y. Cao, J. Wang, and M. Jordan, "Learning transferable features with deep adaptation networks," in *International conference on machine learning*. PMLR, 2015, pp. 97–105. 4
- [29] Y. Sun, L. Zheng, W. Deng, and S. Wang, "Svdnet for pedestrian retrieval," in *Proceedings of the IEEE international conference on computer vision*, 2017, pp. 3800–3808. 6
- [30] A. Dosovitskiy, "An image is worth 16x16 words: Transformers for image recognition at scale," *arXiv preprint arXiv:2010.11929*, 2020. 9
- [31] H. Touvron, M. Cord, M. Douze, F. Massa, A. Sablayrolles, and H. Jégou, "Training data-efficient image transformers & distillation through attention," in *International conference on machine learning*. PMLR, 2021, pp. 10 347–10 357. 9
- [32] W. Chen, X. Xu, J. Jia, H. Luo, Y. Wang, F. Wang, R. Jin, and X. Sun, "Beyond appearance: a semantic controllable self-supervised learning framework for human-centric visual tasks," in *Proceedings of the IEEE/CVF conference on computer vision and pattern recognition*, 2023, pp. 15 050–15 061. 9
- [33] B. Liu, R. Huang, X. Pan, C. Li, J. Sun, J. Dong, and X. Wang, "Advancing ship re-identification in the wild: The shipreid-2400 benchmark dataset and d2internet baseline method," in *Proceedings of the 48th International ACM SIGIR Conference on Research and Development in Information Retrieval*, 2025, pp. 106–115. 9
- [34] H. Liu, X. Tan, and X. Zhou, "Parameter sharing exploration and hetero-center triplet loss for visible-thermal person re-identification," *IEEE Transactions on Multimedia*, vol. 23, pp. 4414–4425, 2020. 9
- [35] C. Fu, Y. Hu, X. Wu, H. Shi, T. Mei, and R. He, "Cm-nas: Cross-modality neural architecture search for visible-infrared person re-identification," in *Proceedings of the IEEE/CVF international conference on computer vision*, 2021, pp. 11 823–11 832. 9
- [36] H. Park, S. Lee, J. Lee, and B. Ham, "Learning by aligning: Visible-infrared person re-identification using cross-modal correspondences," in *Proceedings of the IEEE/CVF international conference on computer vision*, 2021, pp. 12 046–12 055. 9
- [37] Y. Zhang and H. Wang, "Diverse embedding expansion network and low-light cross-modality benchmark for visible-infrared person re-identification," in *Proceedings of the IEEE/CVF conference on computer vision and pattern recognition*, 2023, pp. 2153–2162. 9
- [38] T. Liang, Y. Jin, W. Liu, T. Wang, S. Feng, and Y. Li, "Bridging the gap: Multi-level cross-modality joint alignment for visible-infrared person re-identification," *IEEE Transactions on Circuits and Systems for Video Technology*, vol. 34, no. 8, pp. 7683–7698, 2024. 9
- [39] W.-S. Zheng, J. Yan, and Y.-X. Peng, "A versatile framework for multi-scene person re-identification," *IEEE Transactions on Pattern Analysis and Machine Intelligence*, vol. 47, no. 3, pp. 1362–1380, 2024. 9
- [40] Y. Zhang, Y. Yan, Y. Lu, and H. Wang, "Adaptive middle modality alignment learning for visible-infrared person re-identification," *International Journal of Computer Vision*, vol. 133, no. 4, pp. 2176–2196, 2025. 9
- [41] J. Zhu, H. Ge, Y. Liu, C. Wu, and J. Fan, "Hypergraph-driven soft semantics flexible learning for visible-infrared person re-identification," *Engineering Applications of Artificial Intelligence*, vol. 158, p. 111286, 2025. 9